THE JOURNAL OF BIOLOGICAL CHEMISTRY VOL. 289, NO. 15, pp. 10592–10606 , April 11, 2014
© 2014 by The American Society for Biochemistry and Molecular Biology, Inc. Published in the U.S.A.

Cross-talk between Two Essential Nutrient-sensitive Enzymes

*O-GlcNAc TRANSFERASE (OGT) AND AMP-ACTIVATED PROTEIN KINASE (AMPK)**

Received for publication, September 30, 2013, and in revised form, February 6, 2014 Published, JBC Papers in Press, February 21, 2014, DOI 10.1074/jbc.M113.523068

John W. Bullen[‡], Jeremy L. Balsbaugh[§], Dipanjan Chanda[¶], Jeffrey Shabanowitz[§], Donald F. Hunt[§||], Dietbert Neumann[¶], and Gerald W. Hart[‡1]

From the [‡]Department of Biological Chemistry, The Johns Hopkins University School of Medicine, Baltimore, Maryland 21205, the Departments of [§]Chemistry and [||]Pathology, University of Virginia, Charlottesville, Virginia 22904, and the [¶]Department of Molecular Genetics, Cardiovascular Research Institute Maastricht (CARIM), Maastricht University, 6200 MD Maastricht, The Netherlands

Background: OGT and AMPK collectively target hundreds of intracellular signaling processes, but no study has addressed whether they regulate each other.
Results: AMPK activity mediates the substrate selectivity of OGT, and *O*-GlcNAcylation modulates the activity of AMPK.
Conclusion: There is significant cross-talk between the *O*-GlcNAc and AMPK systems.
Significance: OGT and AMPK may synergistically regulate numerous nutrient-sensitive processes essential for life.

Nutrient-sensitive pathways regulate both *O*-GlcNAc transferase (OGT) and AMP-activated protein kinase (AMPK), cooperatively connecting metabolic homeostasis to regulation of numerous intracellular processes essential for life. Similar to phosphorylation, catalyzed by kinases such as AMPK, *O*-GlcNAcylation is a highly dynamic Ser/Thr-specific post-translational modification of nuclear, cytoplasmic, and mitochondrial proteins catalyzed exclusively by OGT. OGT and AMPK target a multitude of intracellular proteins, with the net effect to protect cells from the damaging effects of metabolic stress. Despite hundreds of studies demonstrating significant overlap in upstream and downstream signaling processes, no study has investigated if OGT and AMPK can directly regulate each other. We show acute activation of AMPK alters the substrate selectivity of OGT in several cell lines and nuclear localization of OGT in C2C12 skeletal muscle myotubes. Nuclear localization of OGT affects *O*-GlcNAcylation of numerous nuclear proteins and acetylation of Lys-9 on histone 3 in myotubes. AMPK phosphorylates Thr-444 on OGT *in vitro*; phosphorylation of Thr-444 is tightly associated with AMPK activity and nuclear localization of OGT in myotubes, and phospho-mimetic T444E-OGT exhibits altered substrate selectivity. Conversely, the α- and γ-subunits of AMPK are *O*-GlcNAcylated, *O*-GlcNAcylation of the γ1-subunit increases with AMPK activity, and acute inhibition of *O*-GlcNAc cycling disrupts activation of AMPK. We have demonstrated significant cross-talk between the *O*-GlcNAc and AMPK systems, suggesting OGT and AMPK may cooperatively regulate nutrient-sensitive intracellular processes that mediate cellular metabolism, growth, proliferation, and/or tissue function.

O-linked β-*N*-acetylglucosamine (*O*-GlcNAc)[2] is a highly dynamic, inducible, and reversible post-translational modification of serine and threonine residues found on over 2500 intracellular proteins involved in the regulation of virtually all core processes associated with cellular metabolism, growth, proliferation, and function. *O*-GlcNAc is essential for life and dysregulated *O*-GlcNAc cycling is involved in the pathogenesis of disorders associated with the metabolic syndrome (*e.g.* cardiovascular disease and type 2 diabetes) and certain types of cancer (1, 2). *O*-GlcNAc cycles on and off Ser/Thr residues by the concerted actions of two enzymes: *O*-GlcNAc transferase (OGT) and *O*-GlcNAcase (OGA), respectively. *O*-GlcNAcylation is a nutrient-sensitive process heavily influenced by flux through the hexosamine biosynthetic pathway (HBP). *De novo* synthesis of uridine diphosphate *N*-acetylglucosamine (UDP-GlcNAc), the high-energy donor substrate for OGT, is heavily dependent on glucose flux through the HBP. Glucose, glutamine, acetyl-CoA, and UTP are all necessary intermediates in UDP-GlcNAc synthesis, suggesting that flux into the HBP may be a mechanism by which intracellular nutrient status is linked to *O*-GlcNAc-specific regulation of hundreds of signaling processes (1, 2).

Similar to *O*-GlcNAcylation, regulation of AMP-activated protein kinase (AMPK) is a vital nutrient-sensing process that mediates cellular and whole body energy homeostasis via dozens or hundreds of protein targets and/or signaling pathways (3). AMPK is a heterotrimeric complex comprising an α (catalytic), and β and γ (regulatory) subunits, with the γ-subunit binding the adenine nucleotides AMP, ADP, and ATP. Each subunit is encoded by multiple genes (α1, α2, β1, β2, γ1, γ2, γ3)

* This work was supported in whole or in part, by National Institutes of Health Grants R01CA42486, R01DK61671, GM037537; N01-HV-00240; P01HL107153, R24DK084949, The Netherlands Organization for Scientific Research VIDI Grant (864.10.007), and the Patrick C. Walsh Prostate Cancer Research Fund.
[1] Beth W. and A. Ross Myers Scholar. To whom correspondence should be addressed: Department of Biological Chemistry, Johns Hopkins University School of Medicine, 725 North Wolfe St., Baltimore, MD. Tel.: 410-614-5993; Fax: 410-614-8804; E-mail: gwhart@jhmi.edu.

[2] The abbreviations used are: *O*-GlcNAc, *O*-linked β-*N*-acetylglucosamine; OGT, *O*-linked β-*N*-acetylglucosaminyltransferase (protein β-*N*-acetylglucosaminyltransferase, EC 2.4.1.94); OGA, *O*-linked β-*N*-acetylglucosaminidase (β-*N*-acetylhexosaminidase, EC 3.2.1.52); ncOGT, nucleocytoplasmic OGT; AMPK, AMP-activated protein kinase; HBP, hexosamine biosynthetic pathway; LKB1, Ser/Thr kinase 11; CAMKKβ, Ca^{2+}/calmodulin-dependent kinase kinase β; ACC, acetyl-CoA carboxylase; FA, fatty acid; GT, 1,2-dideoxy-2′-methyl-α-D-glucopyranoso-[2,1-d]-Δ2′-thiazoline; TMG, 1,2-dideoxy-2′-ethylamino-α-D-glucopyranoso-[2,1-d]-Δ2′-thiazoline; AICAr, aminoimidazole-4-carboxamide riboside; 2DE, 2-dimensional electrophoresis; TPR, tetratricopeptide repeat; HIS, polyhistidine.

generating at least 12 heterotrimeric combinations. AMPK is activated by 5′-AMP and ADP but inhibited by ATP, making it extremely sensitive to intracellular AMP:ATP and ADP:ATP ratios, and thus activated when intracellular energy levels are depleted. AMPK is also responsive to multiple extracellular nutritional and hormonal signals that regulate food intake, energy expenditure, proliferation, and cell viability (3). AMP promotes AMPK activity by two distinct mechanisms, of which the first is also caused by ADP: 1) by promoting increased net phosphorylation of a critical threonine residue (Thr-172) located in the activation loop of the α-subunit, and 2) by allosteric activation of the phosphorylated kinase. In general, activation of AMPK promotes catabolic and inhibits anabolic processes, with net effects to replenish or conserve intracellular ATP. Depending on tissue/cell type, AMPK promotes glucose uptake, glycolysis, and mitochondrial biogenesis, while inhibiting gluconeogenesis, and fatty acid (FA), triglyceride, cholesterol, RNA, and protein synthesis (3). AMPK has thus emerged a strong drug target for disorders associated with the metabolic syndrome and certain types of cancer.

OGT and AMPK collectively target thousands of downstream proteins that vary widely based on biological or experimental parameters and tissue/cell type. A better understanding of non-canonical pathways that mediate contextually dependent spatial, temporal, and/or substrate specific activity of OGT and AMPK is needed. Collectively, data suggest significant overlap in OGT and AMPK signaling processes: First, many metabolic stresses that regulate OGT also regulate AMPK (*e.g.* glucose deprivation, ER stress, and H_2O_2-induced mitochondrial stress). Second, regulation of both OGT and AMPK is associated with protection of cells from the damaging effects of these metabolic stresses. Last, many downstream targets of AMPK are also *O*-GlcNAcylated; *e.g.* CREB-regulated transcription coactivator 2 (CRTC2 or TORC2), cellular tumor antigen (p53), and peroxisome proliferator-activated receptor γ coactivator 1-α (PGC1-α) (4–6). Despite thousands of studies on *O*-GlcNAcylation and AMPK, no study has interrogated the potential for direct dynamic cross-talk between OGT and AMPK. Here, we report that activation of AMPK alters the substrate selectivity of OGT in numerous cell lines and nuclear localization of OGT in differentiated skeletal muscle myotubes, affecting global *O*-GlcNAcylation of nuclear proteins and acetylation of Lys-9 (K9) on histone 3 in myotubes. AMPK phosphorylates Thr-444 (T444) on OGT *in vitro*; phosphorylation of Thr-444 is tightly associated with AMPK activity and increased nuclear localization of OGT in myotubes, and phospho-mimetic Thr-444 to Glu (T444E) mutant OGT exhibits altered substrate selectivity. Conversely, both α- and all 3 γ-subunits of AMPK are *O*-GlcNAcylated, *O*-GlcNAcylation of the γ1-subunit directly correlates with AMPK activity, and acute inhibition of *O*-GlcNAc cycling blunts activation of AMPK by physiological and pharmacological stimuli. Collectively, our results demonstrate significant cross-talk between the *O*-GlcNAc and AMPK systems, suggesting OGT and AMPK may cooperatively regulate nutrient-sensitive intracellular processes essential for life and the pathogenesis of metabolic diseases.

EXPERIMENTAL PROCEDURES

Cell Culture, Treatments, and Transfections—Hek293 and HeLa cells were grown as previously described (7). C2C12 cells were grown in DMEM (4.5 g/liter glucose) supplemented with 20% FBS. Myotube differentiation was induced by incubating 90–95% confluent C2C12 cells in 2% horse serum DMEM for 5–7 days. NAG-thiazoline (GT) and thiamet-G (TMG) were synthesized by custom order (SD ChemMolecules). A-769662 was kindly provided by Dr. Anudharan Balendran (AstraZeneca, Mölndal, Sweden). Cells were treated with GT, TMG, A-769662, or 5-aminoimidazole-4-carboxamide riboside (AICAr) (Enzo Life Sciences) as specified. For nutrient/growth factor deprivation experiments, cells were washed three times with and incubated in Krebs-HEPES buffer (20 mM Na HEPES (pH 7.4), 118 mM NaCl, 3.5 mM KCl, 1.3 mM $CaCl_2$, 1.2 mM $MgSO_4$, 1.2 mM KH_2PO_4, and 25 mM glucose). For glucose deprivation studies in Fig. 2, cells were washed twice with, and incubated in 1 mM glucose DMEM supplemented with dialyzed serum for 2 h. For glucose deprivation studies in Figs. 10 and 11; cells were washed twice with and allowed to recover at 37 °C for 30 min in 0 or 25 mM glucose Krebs-HEPES (0.1% BSA) ± TMG, and incubated in fresh 0.1% BSA Krebs-HEPES supplemented with 0 or 25 mM glucose (± TMG) for the last 1 h prior to lysis. For all studies using AICAr or A-769662, cells were washed three times with, and allowed to recover at 37 °C for 30 min in 0.1% BSA serum-free DMEM (Figs. 2, 3, and 5–8) or 0.1% BSA Krebs-HEPES (Figs. 10 and 11) supplemented with appropriate treatments. Fresh vehicle supplemented with AICAr, A-769662, and/or respective treatments was subsequently added for the indicated times.

Constructs and Recombinant Protein Expression/Purification—Constructs encoding MYC-tagged $\alpha1/\alpha2$, GFP-tagged $\alpha1/\alpha2$, $\beta1/\beta2$, and FLAG-tagged $\gamma1/\gamma2/\gamma3$ subunits of AMPK were kindly provided by Dr. Grahame Hardie (Dundee, UK) (8). Rat EGFP-tagged OGT (in pEGFP-C3 vector; Clontech) was constructed in our laboratory and graciously provided by Drs. Kaoru Sakabe and Quira Zeidan (Baltimore, MD). The construct encoding recombinant full-length human OGT (ncOGT) was kindly provided by Dr. Suzanne Walker (Boston, MA) (24). Mutant EGFP-OGT and ncOGT constructs were generated with QuickChange Lightning Site-directed Mutagenesis (Stratagene) in accordance with the manufacturer's instructions using the forward primers: rat EGFP-OGT (T444A): 5′-CAATAGCTTCTTACCGCGCAGCTCTGAAACTTAAG-3′; human ncOGT (T444A): 5′-GCTTCTTACCGCGCGGCTCTGAAAC-3′; and human ncOGT (T444E): 5′-CATAGCTTCTTACCGCGAGGCTCTGAAACTTAAGC-3′, with their complement reverse primers. Ni^{2+}-purified AMPK $\alpha1\beta1\gamma1$, $\alpha2\beta1\gamma1$, constitutively active mutant AMPK $\alpha1$[T172D]$\beta1\gamma1$, kinase-dead mutant AMPK $\alpha1$[K45R]$\beta1\gamma1$, and ncOGT recombinant proteins were expressed and purified as published (9–11). For Fig. 4*B*, phosphorylation of Thr-172 on the α-subunit and purification of phosphorylated $\alpha1\beta1\gamma1$, $\alpha2\beta1\gamma1$, and mutant $\alpha1$[K45R]$\beta1\gamma1$ was performed as previously published (11). For Fig. 5*A*, phosphorylation of Thr-172 on the α-subunit of $\alpha1\beta1\gamma1$ and mutant $\alpha1$[D157A]$\beta1\gamma1$ was achieved by inducing protein expression

in bacteria transformed with a hexacistronic co-expression plasmid encoding LKB1, MO25α, STRADα, and all three respective AMPK subunits. The hexacistronic plasmid was generated by subcloning a tricistronic co-expression plasmid encoding non-tagged LKB1, MO25α, and STRADα (12) into a tricistronic AMPK expression construct (10). Protein expression induced transformed bacteria were lysed and Ni^{2+}-purification of hexahistidine-tagged pT172-AMPK was subsequently performed as published (10), while the LKB1 complex remained in the flow-through. For a more detailed description of methods used for cloning and purification of hexacistronic plasmid-based pT172-AMPK complexes, please contact Dr. Dietbert Neumann (CARIM, Maastircht University, The Netherlands).

Confocal Microscopy—Proliferating cells were plated on glass coverslips coated with poly-D-lysine (Sigma). To image differentiated C2C12 myotubes, C2C12 cells were plated and differentiated on Thermanox plastic coverslips (Thermo Scientific). Cells were washed, fixed in 4% paraformaldehyde, and processed as published (13). Permeabilized cells were blocked in 5% BSA or 10% goat serum, incubated with antibodies specific for OGT (AL28), OGA (345) (14), H3 K9Ac, and/or H3 K27me3 (Abcam), incubated with the appropriate secondary antibodies (anti-IgG 405-, 488-, 555-, or 647-conjugated Alexa Fluors; Invitrogen) and mounted. For DNA staining, cells were briefly incubated in DAPI (1 μg/ml) before being mounted. Images were captured on a laser scanning Zeiss LSM510-Meta confocal microscope maintained by the Johns Hopkins University microscope core facility. Quantification was performed double blinded (*i.e.* all images were captured and analyzed using coded samples). Confocal images were acquired as a z-stack of five 1-μm slices (spanning a 2.8-μm range). Projections are one representative 1-μm slice. Quantification was performed on the most optimal z-stack for each nucleus. For nuc_{OGT}/$cyto_{OGT}$ measurements, ROI units (2 μm) were placed in the nucleus and immediately adjacent cytoplasm and quantified (ImageJ ROI analysis) to calculate the nuclear-to-cytoplasmic ratio of OGT immunofluorescence. For all quantified data of histone modifications, images were captured in one session using identical microscope settings and nuclear H3 K9Ac or K27me3 immunofluorescence pixel intensities were quantified using ImageJ ROI analyses. $Nuc_{OGT}/Cyto_{OGT}$ distribution curves were generated by counting the number of nuclei exhibiting nuclear-to-cytoplasmic ratios of OGT immunofluorescence that fall within incremental data subsets of 0.2 ranging the maximal dynamic range of the microscope, from 0–4 (*e.g.* 0–0.2, 0.21–0.4, *etc*). The midpoint for each data subset (*e.g.* 0.5 for subset 0.41–0.6) was plotted against the percentage of nuclei exhibiting ratios within the respective data subset and displayed as a smoothed line plot. At least five images were captured/sample for all experiments.

Cell Lysis and Protein Analyses—Cells were lysed off the plate and immediately processed as described (3). Isolation of whole, nuclear, or cytosolic cell lysate, immunoblots, immunoprecipitations, and two-dimensional electrophoresis (2DE) analyses were performed as published (15–18). Briefly, overexpressed mammalian heterotrimeric AMPK complexes were immunoprecipitated from cell lysate using anti-FLAG beads (Sigma). Endogenous AMPK-α2, OGT, and phospho-T444 OGT (pT444-OGT) were immunoprecipitated from cell lysate using antibodies specific for AMPK-α2 (Santa Cruz Biotechnology), OGT (AL28), or pT444-OGT (custom), respectively. For 2DE, 0.5–2 mg of cell lysate was methanol/chloroform precipitated and rehydrated in 8 M urea, 2% CHAPS, 50 mM DTT, and 0.2% BioLyte 3–10 IEF buffer (Bio-Rad). Rehydrated protein samples were swelled onto Readystrip IPG Strips (pI 3–10) (Bio-Rad) at room temperature overnight, isoelectric focused, reduced/carbamidomethylated for 30 min, separated on Criterion pre-cast SDS-polyacrylamide IPG gels (Bio-Rad), transferred to PVDF, and immunoblotted. Protein and phosphorylated protein-specific immunoblots were performed using antibodies specific for the following: AMPK-α1 and -α2 (kindly provided by Dr. Grahame Hardie), AMPK-α, AMPK-β, phospho-T172 on AMPK-α, ACC, phospho-S79 on ACC (Cell Signaling), phospho-T444 on OGT (custom), OGT (AL28), lamin A/C, and myosin heavy chain (Myo_{HC} (Santa Cruz Biotechnology)), FLAG (Sigma), glyceraldehyde 3-phosphate dehydrogenase (GAPDH (Chemicon)), actin (Sigma).

Enrichment for ncOGT-interacting Proteins from Hek293T Lysate—Enrichment for ncOGT-interacting proteins from Hek293T lysate treated with 0.1% DMSO (vehicle) or 100 μM A-769662 for 2 h was performed as described (16), with minor modifications. Briefly, recombinant ncOGT was covalently coupled to CNBr-activated Sepharose 4 Fast Flow beads (GE Healthcare) according to the manufacturer's instructions. Two separate wild-type (WT)- and two separate T444E-ncOGT CNBr columns were prepared. For each column, 3.5 mg of ncOGT was coupled to 1-ml bed volume of CNBr beads. Coupling efficiency was estimated at >99% for all experiments. 100 mg of fresh (never frozen) lysate from either Ctrl or A-769662-treated Hek293T cells was incubated with either WT- or T444E-ncOGT CNBr beads in 20 ml of enrichment buffer (50 mM Tris-HCl (pH 7.4), 50 mM GlcNAc, 50 mM NaF, 5 mM $Na_4P_2O_7$, 1 mM EDTA, 1 mM EGTA, 1 mM dithiothreitol (DTT), 1 mM PMSF, 5 μg/ml soybean trypsin inhibitor, 64 μM benzamidine, 2 μM leupeptin, 3 μM antipain, 10 units/ml aprotinin, and 0.2% (v/v) Triton X-100) at 4 °C overnight. Columns were subsequently washed three times with 10-bed volumes of TBS per wash; and protein was eluted with 8 M urea, dialyzed (in 20 mM Tris-HCl (pH 7.5), 50 mM NaCl), spin concentrated to >3 mg/ml using a Vivaspin (3 kDA MW cut off) protein concentrating spin column (Sartorius), and stored at −20 °C.

AMPK Activity Assays and in Vitro Cold- or [γ^{32}]Phosphate/[^{3}H]GlcNAc Labeling—AMPK activity assays were performed on -α1 or -α2 immunoprecipitates as previously described (8, 15), and data are presented as fold differences in mean specific activity (nanomol of γ-^{32}P incorporated into SAMS peptide/min) normalized to respective controls ± S.E. For *in vitro* [γ^{32}]phosphate or cold ATP labeling, 1 or 500 μg of ncOGT was incubated with 1 or 200 μg of respective AMPK complexes in the presence of 40 μM AMP, 5 mM $MgCl_2$, and 3 μCi [γ-^{32}P]ATP (0.93 μM) or 200 μM ATP in 10 mM HEPES (pH 7.4) for 20–60 min at 37 °C on an orbital shaker (300–500 rpm). For *in vitro* [γ^{32}]phosphate reactions, protein samples were separated by SDS-PAGE, stained with G250 Coomassie Blue, dried, and developed after a 2-h exposure. For cold ATP reactions,

protein samples were processed and immunoblotted as described above. For *in vitro* [^{3}H]GlcNAc-labeling reactions, 5 μg of each respective AMPK complex was incubated with 1 μg of ncOGT, 2 μCi of UDP[^{3}H]GlcNAc, and 0.5 units of Calf intestinal alkaline phosphatase (CIP) in 20 μl of 50 mM HEPES (pH 7.4) overnight at 4 °C on a rotator. Protein samples were subsequently processed as described (16).

Mass Spectrometry—Similar to above, ncOGT and AMPK complexes were incubated with ATP, separated by SDS-PAGE, and gel bands corresponding to the molecular weight of ncOGT were excised for analysis by mass spectrometry. Digestion conditions were similar to those described previously (19). Briefly, excised bands were pH equilibrated in 100 mM NH_4HCO_3, incubated in 10 mM DTT, 55 mM iodoacetamide, 100 mM NH_4HCO_3 to reduce/carbamidomethylate Cys residues, and digested in 12 ng/μl trypsin (Promega) overnight to obtain peptides amenable to mass analysis. Tryptic peptides were extracted from gel slices using alternating washes of 100 mM NH_4HCO_3 and 50% acetonitrile/5% formic acid, followed by a final dehydration in 100% acetonitrile. Tryptic peptides were dried to completion using a Speedvac Concentrator (Savant) and reconstituted in 0.1% acetic acid in water for mass analysis.

For mass spectrometric analyses, a portion of the digest was pressure loaded onto a precolumn (360 μm o.d. × 75 μm i.d.) packed with C18 reverse-phase resin (5–20 μm diameter, 120 Å pore diameter, YMC Co., LTD), desalted with 0.1% acetic acid in water, and connected to an analytical column packed with C18 reverse-phase resin (5-μm diameter, 120 Å pore diameter, YMC Co., LTD) equipped with an integrated electrospray emitter tip (20). Mass analyses were completed on an in-house modified, electron transfer dissociation (ETD)-enabled LTQ-Orbitrap and LTQ-FT-ICR-MS (Thermo Scientific). High resolution MS scans were acquired in the Orbitrap or FT-ICR cell whereas low resolution, data-dependent collision-activated dissociation (CAD) and ETD MS/MS data were acquired in the ion trap using previously described acquisition methods, HPLC gradient and instrument parameters (21). Data analysis was aided using the Open Mass Spectrometry Search Algorithm (OMSSA) (version 2.1.1) to search against a constructed ncOGT (gi 68067509, Accession O15294, NCBI) database using the following variable modifications: oxidation of Met, phosphorylation of Ser, Thr, Tyr, and carbamidomethylation of Cys (22). The remaining OMSSA search parameters have been described previously (21). Peptide MS/MS spectral data pertaining to ncOGT was manually validated by visual inspection of pertinent CAD and ETD spectra. The surface representation of the crystal structure of $hOGT_{4.5}$ complexed with UDP and CKII3K peptide (Protein DataBank ID: 3PE4) (23) was constructed using MacPyMOL Molecular Graphics System (DeLano Scientific).

Phospho-Thr-444 OGT Custom Antibody Design and Purification—Antibody specific for the phosphorylated Thr-444 residue on OGT was custom designed, synthesized, and provided by Pacific Immunology (Ramona, CA). Briefly, naked [C-IPEAIASYR-T-ALKLKPD] and phospho- [C-IPEAIASYR-T(PO3)-ALKLKPD] peptides were synthesized and HPLC purified. Phospho-peptide was coupled to KLH and used as an antigen in 2 separate rabbits. Antibody purification was performed on bleed 11, as previously described (24), with minor modifications. Six 1-ml aliquots of serum were diluted up to 30 ml in 10 mM Tris (pH 7.5), and purified 2× over naked peptide coupled to a Sulfo-link agarose bead column (Thermo Scientific; provided by Pacific Immunology). Flow-through was collected and stored on ice. The naked-peptide column was then washed with 20× bed volumes of 10 mM Tris (pH 7.5) plus 500 mM NaCl, 10× bed volumes of 100 mM glycine (pH 2.5), 15× bed volumes of 10 mM Tris (pH 8.8), 10× bed volumes of 100 mM triethylamine (pH 11.5), and 20–30× bed volumes of 10 mM Tris (pH 7.5). Flow-through was subsequently purified over the naked-peptide column for a third time. Flow-through from this last purification was then purified 2× over the phospho-peptide Sulfo-link column (Thermo Scientific; provided by Pacific Immunology). The phospho-peptide column was subsequently processed as published (24), and antibody aliquots were stored at −20 °C.

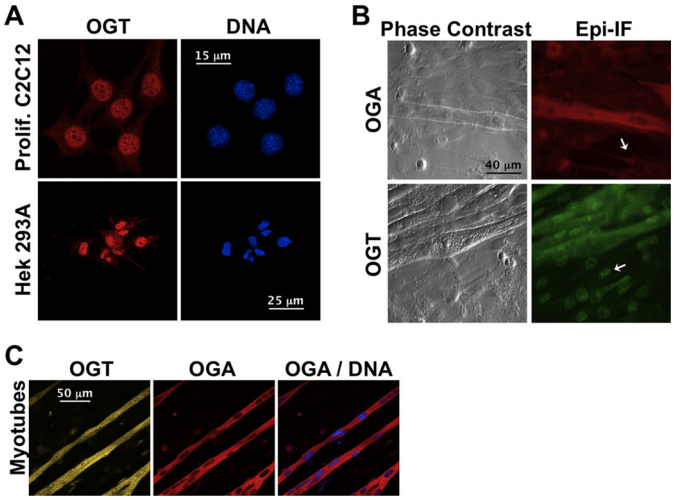

FIGURE 1. **Localization of OGT and OGA in proliferating cells and differentiated C2C12 skeletal muscle cells.** *A*, confocal projections of proliferating C2C12 or Hek293A cells stained for OGT (*red*) and DNA (*blue*). *B*, phase contrast and epi-immunofluorescence (*Epi-IF*) images of differentiated C2C12 cells stained for OGA (*red*) or OGT (*green*). OGA and OGT localization in the myoblastic substrata are indicated (*white arrows*). *C*, confocal projections of C2C12 myotubes stained for OGT, OGA, and DNA.

Statistical Analyses—Quantification of immunoblotted protein band pixel intensities (± S.E.) and densitometric lane profiles were generated using ImageJ software. All data are representative of at least three separate experiments (n = 1 or 2/treatment/experiment), unless otherwise noted. Statistical significance was assessed using ANOVA and standard Student t-tests.

RESULTS

Nuclear Localization of OGT Is Tightly Associated with AMPK Activity in Differentiated C2C12 Mouse Skeletal Muscle Myotubes—To address the potential of direct signaling between *O*-GlcNAc and AMPK systems, we investigated whether acute physiological or pharmacological metabolic stresses known to regulate AMPK also affect protein *O*-GlcNAcylation. We examined the effect of 2 h of glucose deprivation, nutrient/growth factor deprivation (absence of all nutrients except 25 mM glucose (*i.e.* no serum, vitamins, amino acids, sodium pyruvate, or L-glutamine)) and AICAr treatment

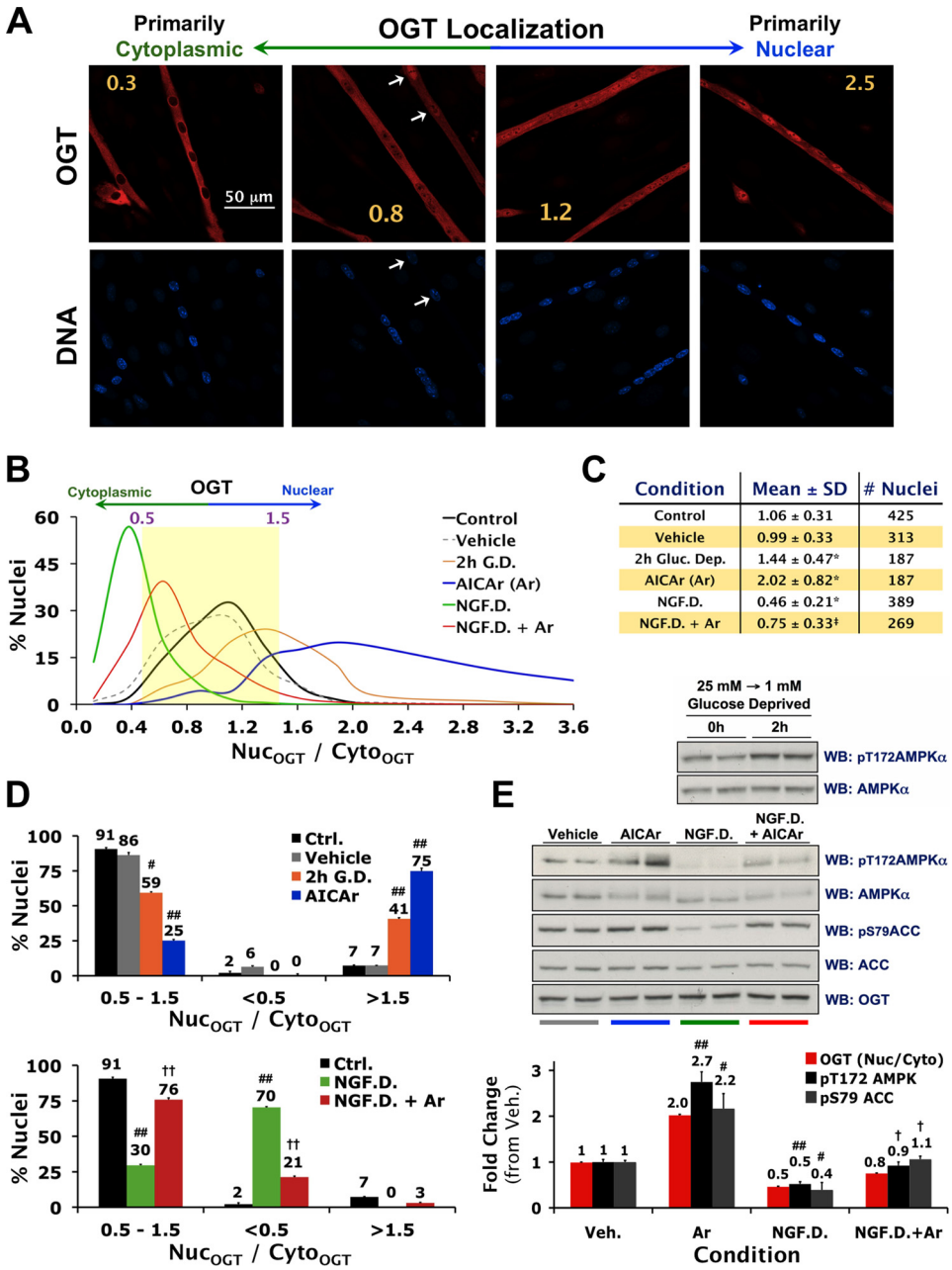

FIGURE 2. **Nuclear localization of OGT is tightly associated with AMPK activity in C2C12 myotubes.** *A*, confocal projections of fixed C2C12 myotubes stained for OGT (*red*) and DNA (*blue*). Nuclear-to-cytoplasmic ratios of OGT immunofluorescence ($Nuc_{OGT}/Cyto_{OGT}$) for each projection are indicated in *yellow*. A high degree of variability in nuclear localization of OGT within the same myotube is indicated with *white arrows*. *B–D*, quantification of $Nuc_{OGT}/Cyto_{OGT}$ values in C2C12 myotubes incubated for 2 h in fresh DMEM (Control or *Ctrl.*), serum-free DMEM (*AICAr vehicle*), 1 mM glucose DMEM (*G.D.*), AICAr (0.5 mM), a buffer deprived of all nutrients/growth factors except 25 mM glucose (*NGF.D.*), or 0.5 mM AICAr in NGF.D. buffer (*NGF.D.+Ar*). *E*, lysates from differentiated C2C12 cells exposed to the same conditions in parallel were immunoblotted (*WB*) as indicated. Mean $Nuc_{OGT}/Cyto_{OGT}$ and densitometric values of phospho- over total AMPK and ACC (±S.E.) are normalized to *Ctrl.* #, ##, and * denote statistical significance of $p < 0.01$, $p < 0.0001$, and $p < 1 \times 10^{-28}$ *versus Ctrl.* and *Veh.*, respectively. †, ††, and ‡ denote statistical significance of $p < 0.01$, $p < 0.001$, and $p < 1 \times 10^{-37}$ *versus NGF.D.*, respectively.

(an AMP-mimetic and routinely used activator of AMPK) on the localization and activity of OGT, OGA, and AMPK in differentiated C2C12 myotubes, the undifferentiated myoblastic cell substrata on which myotubes fuse, and various proliferating cell lines (*e.g.* Hek293A, HepG2, HeLa, and C2C12). Consistent with previous studies (13, 14), in undifferentiated myoblastic cells and all proliferating cell lines studied OGT is primarily localized in the nucleus while OGA is primarily localized in the cytoplasm (Fig. 1, *A* and *B*). In contrast, there is a significant increase in cytoplasmic localization of OGT in differentiated myotubes, while OGA remains primarily cytoplasmic (Fig. 1*C*). These data are consistent with what is observed in other terminally differentiated cell types (*e.g.* rat cerebellar cortex, mouse 3T3-L1 adipocytes, and rat cardiac muscle) (25–27). Collectively, our data and previous work suggest that there are distinct functional roles for OGT in differentiated *versus* proliferating cells.

Under basal conditions, OGT exhibited a broad bell curve-shaped percent distribution of nuclear-to-cytoplasmic ratios of OGT immunofluorescence ($nuc_{OGT}/cyto_{OGT}$) in myotubes. This was due to the high degree of variability in nuclear local-

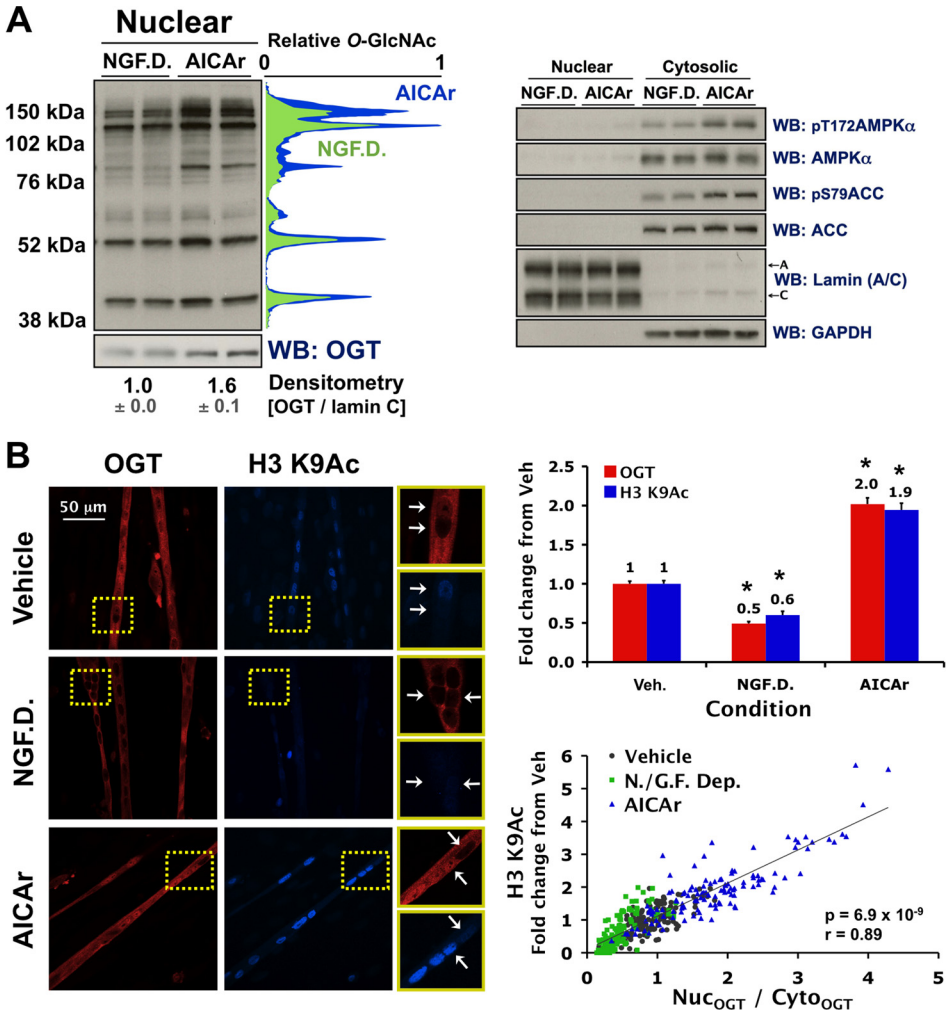

FIGURE 3. **Nuclear localization of OGT correlates with *O*-GlcNAcylation of nuclear proteins and H3 Lys-9 acetylation in C2C12 myotubes.** *A*, cytosolic and/or nuclear extracts from differentiated C2C12 cells subjected to 2 h of NGF.D. or 0.5 mM AICAr were immunoblotted (*WB*) for *O*-GlcNAcylated protein, OGT, and controls as indicated, including lamin (*A/C*) (nuclear loading control) and GAPDH (cytosolic loading control). Quantified densitometric lane profiles (relative scale of 0 to 1) of the representative *O*-GlcNAc WB were normalized to lamin C (NGF.D. (*green*), AICAr (*blue*)). *B*, confocal projections of fixed C2C12 myotubes incubated for 2 h in vehicle, NGF.D. buffer, or AICAr (0.5 mM), and stained for OGT (*red*) and H3 K9Ac (*blue*). Examples of correlation between OGT and H3 K9Ac nuclear staining for each condition are cropped (*yellow boxes*), blown up (*right panels*), and indicated with *white arrows*. Correlative and mean value (± S.E.) quantification of the nuclear-to-cytoplasmic ratios of OGT immunofluorescence ($Nuc_{OGT}/Cyto_{OGT}$) and H3 K9Ac nuclear immunofluorescence (normalized to vehicle; *Veh.*) are plotted (>120 nuclei/condition). * denotes statistical significance of $p < 1 \times 10^{-20}$ *versus Veh*.

ization of OGT both between myotubes and within the same myotube (Fig. 2*A*). In general, there was relatively equal nuclear and cytoplasmic localization of OGT, with a mean $nuc_{OGT}/cyto_{OGT}$ ratio of 1.06 and over 90% of the nuclei exhibiting $nuc_{OGT}/cyto_{OGT}$ ratios between 0.5 and 1.5 (Fig. 2, *B--D*). Two hours of glucose deprivation, a mild physiological activator of AMPK, increased nuclear localization of OGT. Treatment with AICAr, a more specific pharmacological activator of AMPK (15), induced a dramatic increase in nuclear localization of OGT, with 75% of the nuclei exhibiting $nuc_{OGT}/cyto_{OGT}$ ratios greater than 1.5 (Fig. 2, *B–D*). An effect similar to what was observed with glucose deprivation was observed after just 30 min of AICAr treatment (mean $nuc_{OGT}/cyto_{OGT}$ value of $1.46 \pm 0.53, p < 1 \times 10^{-11}$). In contrast, nutrient/growth factor deprivation (in the presence of 25 mM glucose) induced a dramatic decrease in nuclear localization of OGT, with 70% of the nuclei exhibiting $nuc_{OGT}/cyto_{OGT}$ ratios less than 0.5 (Fig. 2, *B–D*). AICAr rescued nutrient/growth factor deprivation-induced decreases in nuclear localization of OGT (Fig. 2, *B–D*). AMPK activity in lysate from differentiated C2C12 cells treated in parallel directly correlated with nuclear localization of OGT in myotubes (assessed by immunoblotting for phospho-Thr-172 AMPK-α and phospho-Ser-79 on acetyl-CoA carboxylase (ACC, a ubiquitous downstream target of AMPK)) (Fig. 2*E*). Importantly, activation of AMPK had no effect on the enzymatic activity of OGT, the localization of OGT in proliferating cells and undifferentiated myoblastic cells, or the localization of OGA in all cell lines. Our data demonstrate that nutrient-sensitive nuclear localization of OGT is tightly associated with AMPK activity in myotubes.

Nuclear Localization of OGT Correlates with O-GlcNAcylation of Nuclear Proteins and Acetylation of Lys-9 on Histone 3 in Myotubes—OGT has a myriad of downstream targets and functional roles in the nucleus (2, 6). We therefore wanted to confirm that altered localization of OGT by nutrient deprivation and AICAr is consistent with global changes in

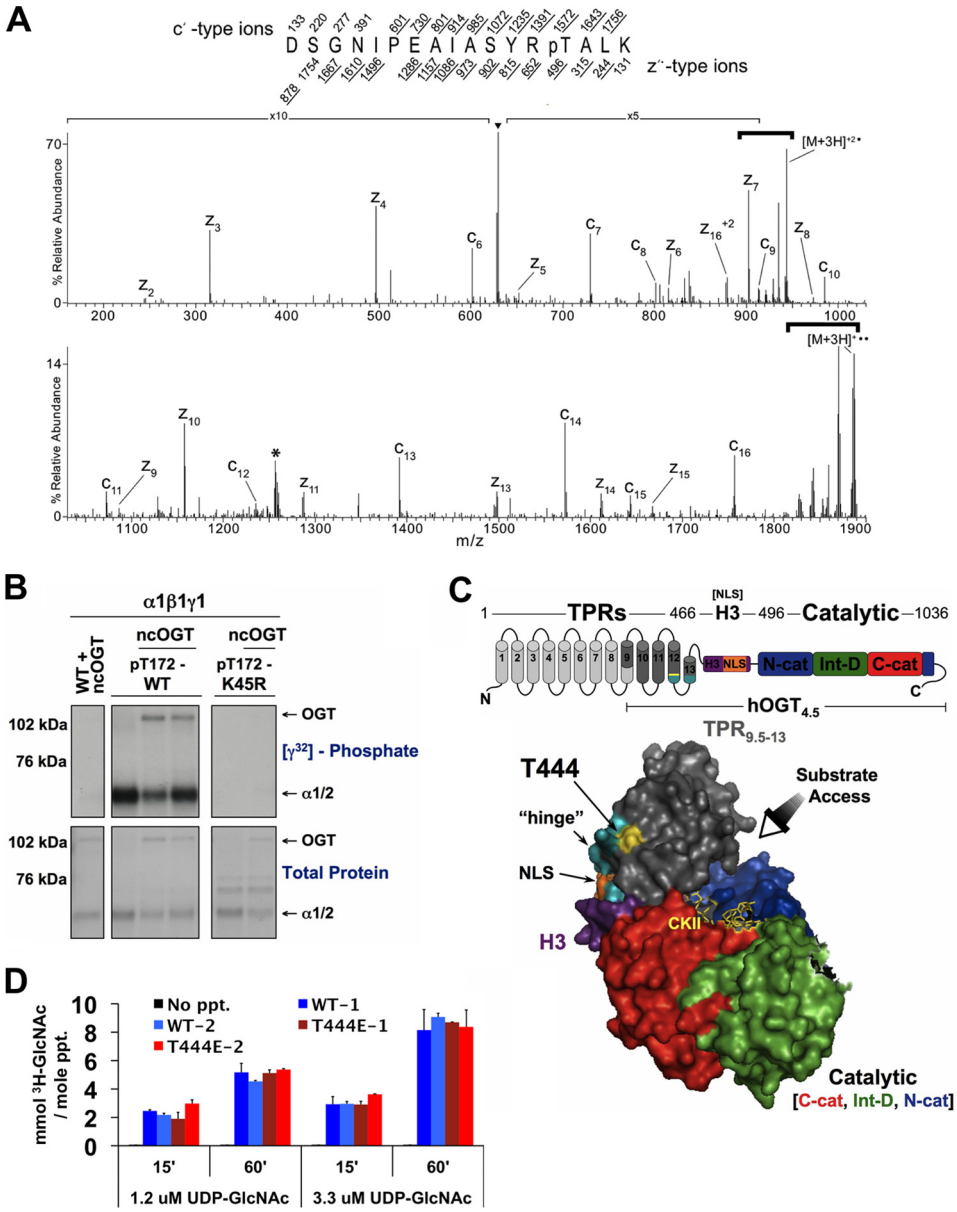

FIGURE 4. **AMPK phosphorylates Thr-444 on OGT *in vitro*.** *A*, ETD MS/MS spectra of $[M+3H]^{3+}$ ions (*m/z* 629.6) of the phosphorylated ncOGT peptide, DSGNIPEAIASYRpTALK. Two ETD spectra were averaged to obtain this spectrum. The predicted monoisotopic c′ and z′-type fragment ion masses are listed above and below the peptide sequence, respectively. The predicted average mass for the doubly charged z_{16} ion is shown. All fragment ions identified within the spectrum are labeled while the corresponding predicted ion masses are *underlined* within the peptide sequence. Reduced charge species resulting from electron capture without dissociation are labeled within the spectrum with neutral losses from these species contained by *heavy brackets*. Species that fall within the prescribed 3 Da isolation window are represented by ▼, whereas those denoted with an *asterisk* correspond to reduced charge species resulting from a coeluting, doubly charged species. *B*, wild-type (WT), phosphorylated active wild-type (*pT172-WT*), or phosphorylated kinase-dead mutant (*pT172-K45R*) recombinant AMPK-α1β1γ1 complexes were incubated with recombinant *O*-GlcNAc transferase (*ncOGT*) in the presence of [γ-^{32}P]ATP (an autoradiograph ([γ^{32}]phosphate; *top panels*) of the same gel stained with G250 Coomassie Blue (total protein; *bottom panels*)). *C*, location of Thr-444 (*yellow*) on a surface representation of the crystal structure of $hOGT_{4.5}$ complexed with UDP and CKII peptide (*stick structure* in the substrate-binding cleft of OGT). $hOGT_{4.5}$ contains a truncated TPR domain (4.5 TPR units; *gray*) connected to the catalytic domain (N-terminal catalytic (N-cat; *blue*), intervening (Int-D; *green*) and C-terminal catalytic (C-cat; *red*) subdomains) via a transitional helix (H3; *purple*) which includes a predicted nuclear localization signal (NLS; *orange*). Pivoting about the hinge (represented as the last 6 amino acids of TPR 12 and first 6 amino acids of TPR 13 in *teal*) is postulated to facilitate access of a wide variety of substrates to the substrate-binding cleft of OGT. *D*, OGT activity assays of 2 separate purifications of recombinant WT- and T444E-ncOGT. Assays performed on no CKII peptide (*No ppt.*) were included as negative controls.

O-GlcNAcylation of nuclear proteins, and altered regulation of a nuclear process previously reported to be regulated by OGT. Immunoblots of nuclear extracts from differentiated C2C12 cells deprived of nutrients and growth factors or treated with AICAr demonstrated a strong association between *O*-GlcNAcylation of nuclear proteins and AMPK activity (Fig. 3*A*). Notably, biochemical analyses of lysate from differentiated C2C12 cells include cellular extract from the unresponsive myoblastic substrata in which OGT is primarily nuclear (Fig. 1*B*). The observed 1.6-fold difference in nuclear OGT assayed by immunobloting (Fig. 3*A*), *versus* approximate 4-fold difference in nuclear OGT assayed by microscopy in myotubes under the same conditions (Fig. 2) exemplifies this concept. The observed changes in *O*-GlcNAcylation of total nuclear extract

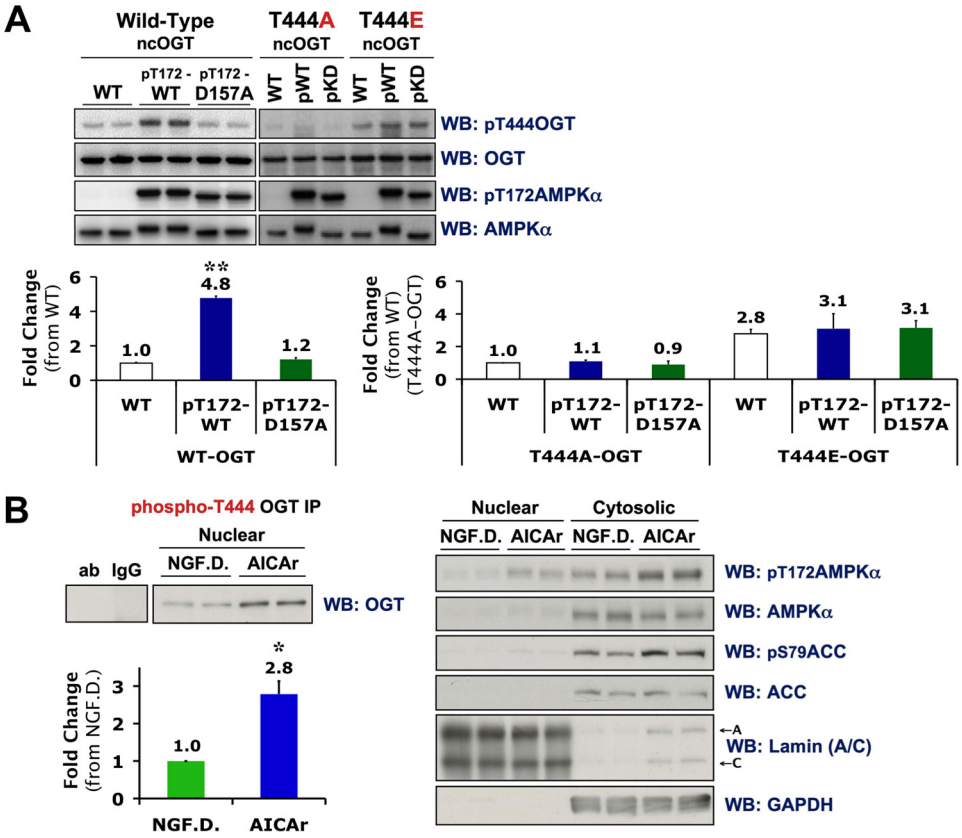

FIGURE 5. **Phosphorylation of Thr-444 on OGT is tightly linked with AMPK activity and nuclear localization of OGT in C2C12 myotubes.** *A,* wild-type (*WT*), phosphorylated active wild-type (pT172-WT or pWT), or phosphorylated kinase dead mutant (pT172-D157A or pKD) recombinant AMPK-$\alpha1\beta1\gamma1$ complexes were incubated with WT, T444A mutant or T444E phospho-mimetic ncOGT in the presence of ATP and immunoblotted (*WB*) as indicated. Densitometric quantification (mean value ± S.E.) of phospho-Thr-444 OGT over total OGT immunoblots was normalized to respective *WT* controls. *B, left panel,* phospho-Thr-444 OGT immunoprecipitates (*IP*) of nuclear extracts from differentiated C2C12 cells subjected to 2 h of NGF.D. or 0.5 mM AICAr were immunoblotted for OGT. Primary antibody incubated without nuclear lysate (*ab*) and lysate incubated with nonspecific IgG (*IgG*) were included as negative controls. Densitometric quantification (mean value ± S.E.) of OGT immunoblots are normalized to *NGF.D. Right panel,* control immunoblots, including lamin (*A/C*) (nuclear loading control) and GAPDH (cytosolic loading control), of nuclear and cytosolic extracts used for immunoprecipitations. * and ** denote statistical significance of $p < 1 \times 10^{-8}$ and $p < 1 \times 10^{-10}$, respectively.

are likely representative of a more significant difference in *O*-GlcNAcylation of nuclear proteins specifically in myotubes.

To confirm that nuclear localization of OGT in myotubes affects a nuclear process previously reported to be regulated by OGT in other cell lines (*e.g.* histone modifications) (2, 6), we used confocal microscopy to investigate the effect of nutrient/growth factor deprivation or AICAr on acetylation of Lys-9 (K9Ac) and tri-methylation of Lys-27 (K27me3) on histone 3 (H3). H3 K9Ac levels were significantly decreased with nutrient/growth factor deprivation and increased with AICAr (Fig. 3*B*). H3 K9Ac levels were highly correlated with nuclear localization of OGT, not only between myotubes, but within the same myotube for each condition (Fig. 3*B*), demonstrating that acetylation of Lys-9 on histone 3 is tightly linked to the presence of OGT in the nucleus. There was no effect of nutrient/growth factor deprivation or AICAr on H3 K27me3 levels. Our data demonstrate that acute metabolic stresses that alter AMPK activity affect nuclear localization of OGT, *O*-GlcNAcylation of nuclear proteins and acetylation of Lys-9 on H3 in myotubes.

AMPK Phosphorylates Thr-444 on OGT in Vitro, and Phosphorylation of Thr-444 Is Tightly Linked to AMPK Activity and Increased Nuclear Localization of OGT in Myotubes—Many plausible mechanisms could account for the effects of nutrient/growth factor deprivation and AMPK activity on the localization of OGT. To assess if phosphorylation of OGT by AMPK is one possibility, we incubated recombinant nucleocytoplasmic OGT (ncOGT) with phosphorylated fully active recombinant AMPK (pT172-WT) in the presence of [γ-^{32}P]ATP. Using tandem mass spectrometry, we identified Thr-444 as the residue on OGT phosphorylated by AMPK *in vitro* (Fig. 4, *A* and *B*). Full-length OGT is composed of a C-terminal catalytic domain and 13 N-terminal tetratricopeptide repeats (TPR). Based on a combination of experimental data and computational molecular modeling, Lazarus *et al.* proposed that OGT dramatically pivots about a "hinge" region located between TPR repeats 12 and 13, facilitating access of a wide variety of potential targets to the substrate binding cleft of OGT (23). A predicted nuclear localization signal (NLS) (2) is located directly adjacent to the "hinge" region. Thr-444 is located at the C-terminal distal end of TPR 12, in close proximity to the "hinge" region (Fig. 4*C*) congruent with the possibility that phosphorylation of Thr-444 by AMPK could regulate both the nuclear localization and substrate selectivity of OGT. Consistent with our data, there was no difference in the enzymatic activity between wild-type (WT) and phospho-mimetic T444E-ncOGT (Fig. 4*D*).

To determine if Thr-444 regulates AMPK-induced nuclear localization of OGT in cell culture, we investigated the localization of overexpressed GFP-tagged WT and Thr-444 to Ala

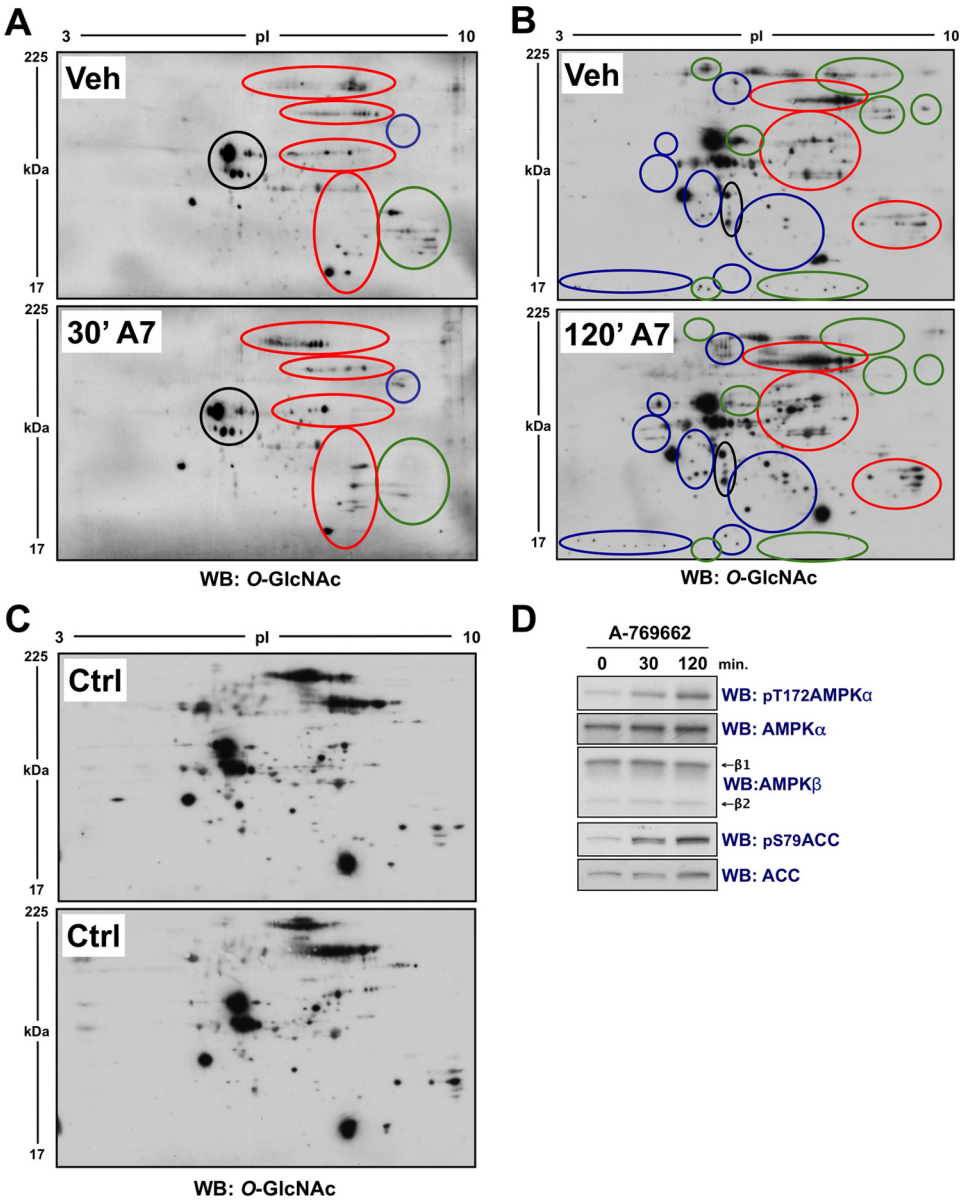

FIGURE 6. **Highly specific activation of AMPK alters global *O*-GlcNAcylated protein status in proliferating cells.** *A* and *B*, lysates from proliferating Hek293T cells incubated for 30 min (*A*) or 120 min (*B*) in vehicle (*Veh*; 0.1% DMSO in serum-free DMEM) or A-769662 (A7; 0.1 mM) were separated by two-dimensional electrophoresis (*2DE*) and immunoblotted (*WB*) for *O*-GlcNAcylated protein. *Blue, green*, and *red circles* highlight regions where A-769662 generally increased, decreased, or altered *O*-GlcNAcylated protein patterning, respectively. The *black circle* highlights a region that does not change, as reference for equal loading. *C, O*-GlcNAc immunoblots of untreated lysate from Hek293T cells processed and analyzed in parallel (analogous to data presented in *A* and *B*) confirms a low degree of intra-experimental variability. *D,* control immunoblots of the same lysate used for both the 30- and 120-min time points confirm time-dependent activation of AMPK.

(T444A) mutant OGT in various proliferating cell lines and differentiated C2C12 cells. In contrast to what is observed with endogenous OGT expression (Fig. 1), overexpressed OGT is primarily cytoplasmic in proliferating cells and virtually excluded from the nucleus in myotubes (data not shown[3]). The mechanisms driving disrupted localization of overexpressed OGT in cell culture remains unknown, but is consistent with previous literature in which a very small increase in OGT expression (2–3-fold) has profound effects on multiple signaling pathways (13). These data indicate that studies investigating AMPK-mediated regulation of overexpressed OGT in cells are not physiologically relevant.

To assess if activation of AMPK could alter phosphorylation of Thr-444 on endogenous OGT in cell culture, we designed a custom antibody specific for phosphorylated Thr-444 on OGT. Phospho-Thr-444 OGT immunoblots of recombinant WT, T444A mutant, and T444E phospho-mimetic ncOGT incubated with or without phosphorylated active recombinant (pT172-WT) or phosphorylated kinase-dead mutant (pT172-D157A) AMPK in the presence of ATP confirmed antibody specificity for phospho-Thr-444 over naked OGT (Fig. 5*A*). Although specific, technical caveats render this antibody unsuitable for immunofluorescence, or immunoblotting of cell lysate and OGT immunoprecipitates. However, we observed an approximate 3-fold increase in the amount of phospho-Thr-444 OGT immunoprecipitated from nuclear extracts of differentiated C2C12 cells treated with AICAr *versus* nutrient/growth factor deprivation (Fig. 5*B*). We expect this effect would

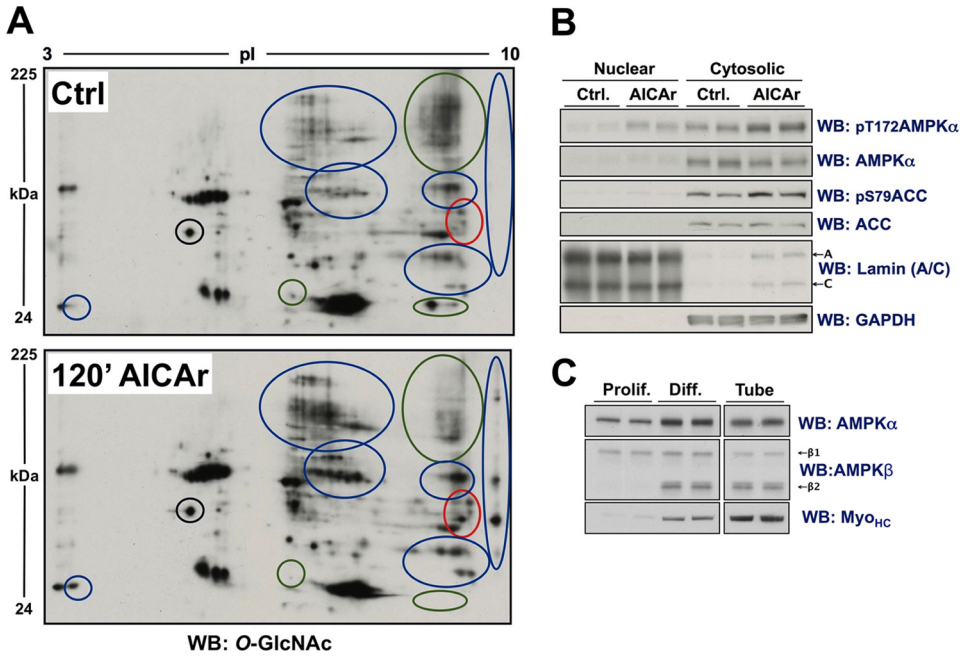

FIGURE 7. **AICAr-induced activation of AMPK in differentiated C2C12 cells alters *O*-GlcNAcylated protein immunoblot patterning of the cytosolic fraction of lysates separated by 2DE.** *A,* the cytosolic fraction of lysates from differentiated C2C12 cells treated with vehicle (*Ctrl.*) or AICAr (0.5 mM, 120 min) were separated by two-dimensional electrophoresis (*2DE*) and immunoblotted (*WB*) for *O*-GlcNAcylated protein. *Blue, green*, and *red circles* highlight regions where AICAr generally increased, decreased, or altered *O*-GlcNAcylated protein patterning, respectively. The *black circle* highlights a region that does not change, as reference for equal loading. *B,* control immunoblots, including lamin (*A/C*) (nuclear loading control) and GAPDH (cytosolic loading control), of the nuclear and cytosolic fractions of the same lysates presented in *panel A* confirms activation of AMPK. *C,* lysates from proliferating (*Prolif.*) and differentiated (*Diff.*) C2C12 cells, and lysate from myotubes enriched from differentiated C2C12 cells (*Tube*) were immunoblotted as indicated (myosin heavy chain (Myo_{HC}; myotube marker)), confirming β2-subunit harboring AMPK complexes as the predominantly expressed isoenzyme in myotubes.

have been- more significant if it were possible to perform these immunoprecipitations on lysate from isolated myotubes, decreasing noise from the unresponsive myoblastic substrata. Collectively, our data indicate nuclear localization of OGT could be mediated by direct phosphorylation of Thr-444 by AMPK in myotubes.

The Substrate Selectivity of OGT Is Altered by Highly Specific Activation of AMPK in Proliferating Cells and Phospho-mimetic Mutation of Thr-444 (T444E) in Vitro—Although there was no effect any of the conditions tested on the localization of OGT in proliferating cells, because the location of Thr-444 is near the proposed "hinge" region, we speculated there might be an effect on the substrate selectivity of OGT. There are over 2500 *O*-GlcNAcylated proteins, making analysis of global changes in the substrate selectivity of OGT by conventional one-dimensional SDS-PAGE not suitable. We exploited two-dimensional electrophoresis (2DE) to separate protein by both mass and charge, facilitating a more accurate global analysis of altered *O*-GlcNAcylated protein status in the cell.

Acute treatment (0.5 and 2 h) with a highly specific small molecule activator of β1-subunit harboring AMPK complexes, A-769662 (28), induced global changes in protein *O*-GlcNAcylation in proliferating Hek293T cells (Fig. 6). Similar results were observed in HepG2 and proliferating C2C12 cells. Activation of AMPK using AICAr also altered global protein *O*-GlcNAcylation in the cytosolic fraction of lysate from differentiated C2C12 cells (Fig. 7, *A* and *B*). Although nonspecific effects are unlikely when using AICAr within a short time frame (*i.e.* within 30 min) (15), siRNA-mediated knockdown of AMPK in the presence of AICAr, or the use of a highly specific activator of AMPK (*e.g.* A-769662) would provide more conclusive evidence supporting AMPK-dependent regulation of OGT in myotubes. Two technical caveats prevent use of these approaches in differentiated C2C12 cells: One, viral infection of C2C12 myotubes requires 72 h of incubation in high-titer lentivirus (>200 MOI), affecting *O*-GlcNAcylation irrespective of AMPK activity. Two, β2-subunit harboring AMPK complexes are primarily expressed in differentiated C2C12 myotubes (Fig. 7*C*), rendering studies with A-769662 in these cells not feasible. Despite these caveats, data discussed thus far occurs within a time scale consistent with the potential for direct signaling between AMPK and OGT (*i.e.* 0.5 to 2 h), and recent data suggest that *O*-GlcNAcylated protein substrate specificity is largely mediated by OGT, *versus* OGA (29).

To determine if the effects of AMPK activation on the substrate selectivity of OGT could be mediated by phosphorylation of Thr-444, we investigated differences in enrichment for WT-*versus* T444E-ncOGT interacting proteins from lysate of Hek293T cells incubated in A-769662 for 0 or 2 h. Significant global changes in *O*-GlcNAcylated proteins bound to WT- *versus* T444E- ncOGT (Fig. 8, *A* and *B*) demonstrate placement of a large highly charged moiety on residue Thr-444 (analogous to phosphorylation) is sufficient to induce dramatic changes in the substrate selectivity of OGT. A significant increase in enrichment for AMPK from A-769662 conditioned lysate (Fig. 8*C*) is congruent with all other data presented demonstrating increased interaction between OGT and activated AMPK.

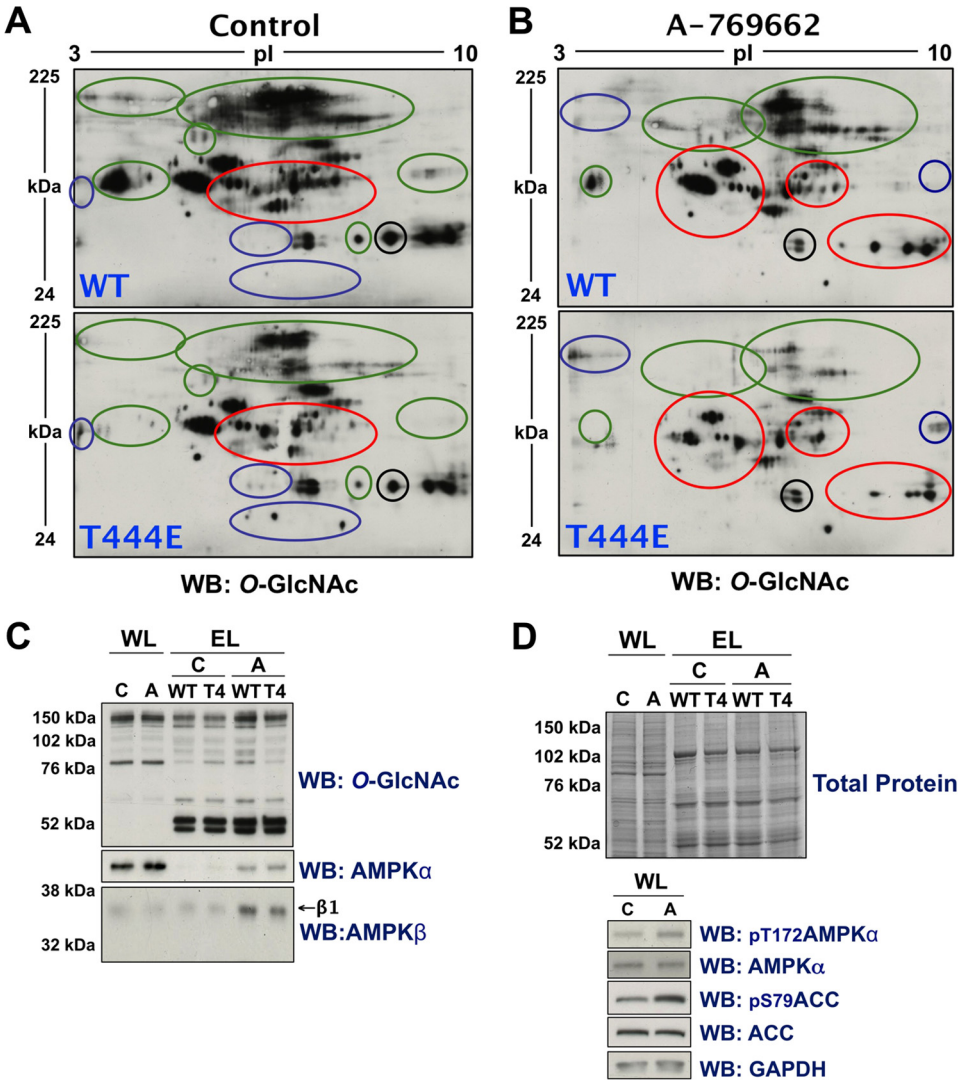

FIGURE 8. **Phospho-mimetic (T444E) recombinant ncOGT exhibits altered substrate selectivity.** *A* and *B*, lysates from Hek293T cells incubated for 2 h in either vehicle (Control; 0.1% DMSO in serum-free DMEM) (*A*) or A-769662 (0.1 mM) (*B*) were enriched for either WT or T444E ncOGT-interacting proteins, separated by two-dimensional electrophoresis and immunoblotted (*WB*) for *O*-GlcNAcylated protein. *Blue, green* and *red circles* highlight regions where *O*-GlcNAcylated protein patterning is generally increased, decreased, or altered, respectively. The *black circle* highlights a region that does not change, as reference for equal loading. *C*, whole-cell lysates (*WL*) and enriched lysates (*EL*) from the experiments used in *panels A* and *B* were immunoblotted for *O*-GlcNAcylated protein, and the α- and β-subunits of AMPK. *D*, *top panel*, G250 Coomassie Blue staining (*Total Protein*) and *bottom panel*, control immunoblots of WL and EL confirm equal loading and activation of AMPK, respectively.

The α (Catalytic) and γ (Regulatory) Subunits of AMPK Are Dynamically O-GlcNAcylated—To demonstrate cross-talk between the *O*-GlcNAc and AMPK systems, *versus* unidirectional regulation of *O*-GlcNAcylation by AMPK, we first determined if AMPK is *O*-GlcNAcylated. The α1-, α2-, and γ1-subunits of recombinant AMPK were *O*-GlcNAcylated by ncOGT *in vitro* (Fig. 9*A*). Overexpressed α1, α2-, γ1-, γ2-, and γ3-subunits of AMPK were *O*-GlcNAcylated in Hek293A cells. Interestingly, the α-subunits were only modified in complexes harboring the γ1-subunit (Fig. 9*B*). The endogenous α-subunit of AMPK was *O*-GlcNAcylated and co-immunoprecipitated with the β1- and β2-subunits in Hek293 and HeLa cells (Fig. 9, *C* and *D*), consistent with what was observed with overexpressed protein. Importantly, increased *O*-GlcNAcylation of the α-subunit after 6 h of treatment with GT, an inhibitor of OGA (Fig. 9*D*) (30), suggests *O*-GlcNAc cycles on and off the α-subunit under basal conditions, and thus may play a role in regulating AMPK during maintenance of cellular homeostasis.

To assess the possibility of a functional role for *O*-GlcNAc on AMPK, we examined whether *O*-GlcNAcylation of the α- or γ-subunits is altered by treatment with AICAr or glucose deprivation. Treatment of Hek293A cells with AICAr induced a 2-fold increase in *O*-GlcNAcylation of the γ1-subunit of AMPK (Fig. 10*A*). There is also a progressive increase in *O*-GlcNAcylation of the γ1-subunit after 3, 6, and 12 h of glucose deprivation (Fig. 10*B*). Consistent with previous publications (16), global increases in OGT and *O*-GlcNAcylated protein was only observed after 12 h of glucose deprivation. *O*-GlcNAcylation of the γ1-subunit by recombinant ncOGT was increased on phosphorylated active wild-type (pT172-WT) and constitutively active (T172D) AMPK, but not on phosphorylated kinase-dead (pT172-K45R) AMPK *in vitro*

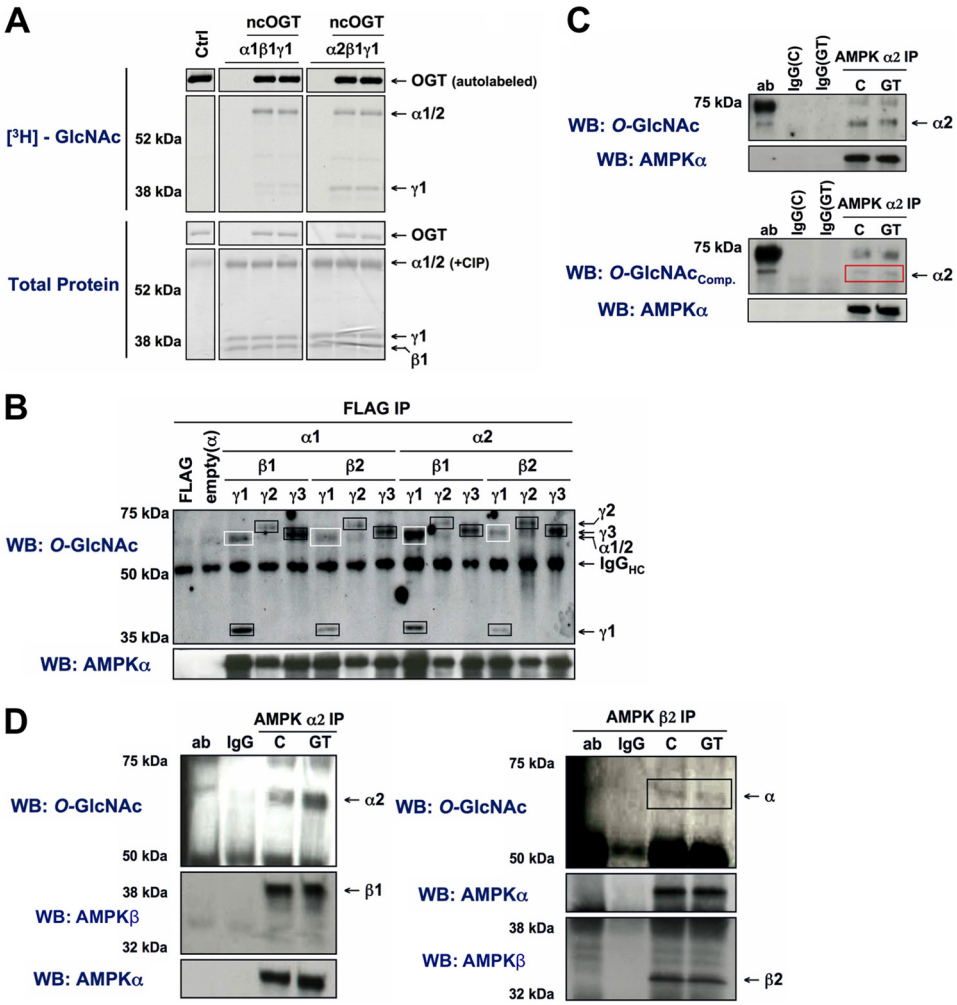

FIGURE 9. **The α1-, α2-, γ1-, γ2-, and γ3-subunits of AMPK are *O*-GlcNAcylated.** *A*, recombinant AMPK-α1β1γ1 or -α2β1γ1 complexes were incubated with recombinant *O*-GlcNAc transferase (ncOGT) in the presence of UDP-[^{3}H]-GlcNAc [an autofluorograph ([^{3}H]-GlcNAc; *top panel*) of the same gel stained with G250 Coomassie Blue (Total Protein; *bottom panel*)]. Reactions without AMPK (*Ctrl*) or ncOGT were included as negative controls. *B*, 12 possible AMPK heterotrimeric combinations of Myc-α1/2, β1/2, and γ1/2/3-FLAG were co-expressed in Hek293A cells and immunoprecipitated (*IP*) with anti-FLAG beads. IPs were immunoblotted (*WB*) for *O*-GlcNAcylated protein and AMPK-α. Anti-FLAG beads incubated without cell lysate (FLAG), and anti-FLAG IPs of cells expressing an empty (α) vector were included as negative controls. *White boxes* and *black boxes* outline bands corresponding to *O*-GlcNAcylated α- and γ-subunits, respectively. *C*, AMPK-α2 immunoprecipitates from Hek293A cells treated with vehicle (*C*) or GT (10 μM, 2 h) were immunoblotted for *O*-GlcNAcylated protein (CTD 110.6) and AMPK-α. Competition of CTD 110.6 antibody reactivity by 1 M GlcNAc (*lower panel*) confirms the specificity of the antibody for *O*-GlcNAcylated protein. The *red box* highlights where nonspecific CTD 110.6 reactivity of the α2-subunit would be. Primary antibody incubated without cell lysate (*ab*) and lysate incubated with nonspecific IgG (IgG) were included as negative controls. *D*, AMPK-α2 or -β2 immunoprecipitates of HeLa cells treated with vehicle (*C*) or GT (10 μM, 6 h) were immunoblotted for *O*-GlcNAcylated protein, AMPK-α and AMPK-β. The *black box* highlights *O*-GlcNAcylated α-subunit co-immunoprecipitated with β2. Primary antibody incubated without cell lysate (*ab*), and lysate incubated with nonspecific IgG (*IgG*) were included as negative controls.

(Fig. 10*C*). Taken together, our data demonstrates both α- and all 3 γ-subunits of AMPK are *O*-GlcNAcylated, that *O*-GlcNAcylation of the γ1-subunit correlates with AMPK activity, and that targeting proteins are not necessary for increased *O*-GlcNAcylation of the γ1-subunit upon activation of AMPK.

Acute Inhibition of O-GlcNAc Cycling Blunts Activation of AMPK in Differentiated Muscle Cells—Next, we determined if acute global perturbation of *O*-GlcNAc cycling has any effect on physiological and pharmacological activation of AMPK. Acute treatment with a highly specific inhibitor of OGA, TMG (31) inhibited glucose deprivation-induced phosphorylation of Thr-172 on AMPK and blunted phosphorylation of Ser-79 on ACC (Fig. 11, *A* and *B*). Inhibition of OGA increased basal phosphorylation of AMPK after prolonged (8 h) treatment, but there was no effect on phosphorylation of ACC (Fig. 11*B*) suggesting this may be a compensatory mechanism for global dampening of phosphorylated active AMPK. Pre-treatment of differentiated C2C12 cells for 2 h with GT (a less specific inhibitor of OGA compared with TMG) blunted AICAr-induced increases in the kinase activity of AMPK-α1 and -α2 immunoprecipitates (Fig. 11*C*), but had no effect on phosphorylation of Thr-172. We speculate supra-physiological activation of AMPK with AICAr, which leads to very rapid and dramatic increases in intracellular AMP, overcomes the effect of acute inhibition of *O*-GlcNAc cycling on phosphorylation of Thr-172. The observed reduction in immunoprecipitated AMPK-α1 kinase activity is therefore independent of phosphorylation of Thr-172, and is congruent with *O*-GlcNAc dampening the activity of phosphorylated active AMPK. Control data collectively demonstrated; One, global elevation of *O*-GlcNAcylated proteins for all experiments using TMG or GT confirmed inhibition of OGA. Two, treatment with TMG or GT for up to 48h had

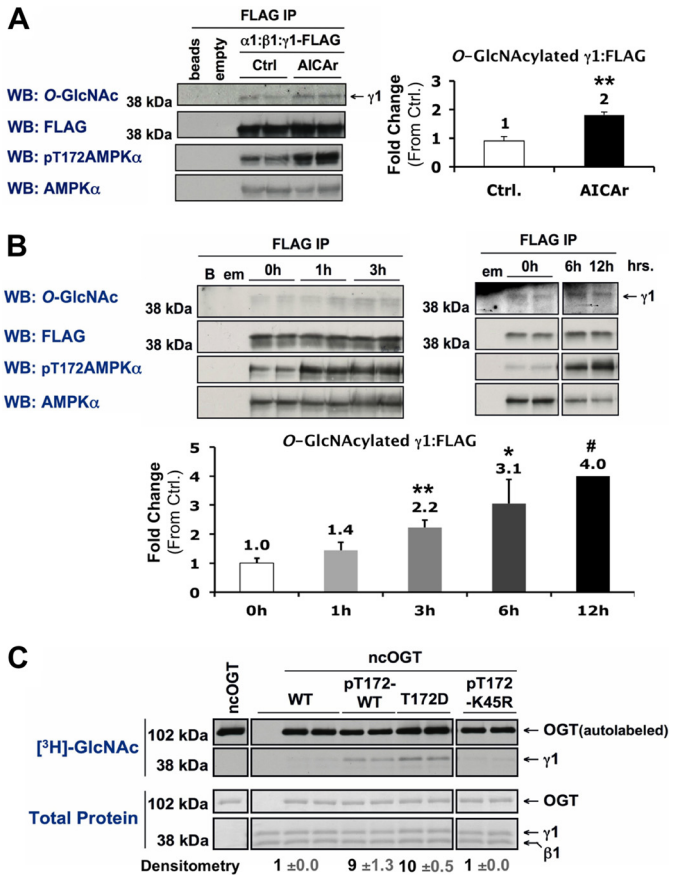

FIGURE 10. **Activation of AMPK increases *O*-GlcNAcylation of its γ1-subunit.** *A* and *B*, *Myc*-α1, β1, and γ1-FLAG constructs were co-expressed in Hek293A cells incubated in vehicle (*Ctrl*) or AICAr (1 mM, 2 h) (*A*), or 0 mM glucose for 0, 1, and 3 h or 0, 6, and 12 h (*B*). AMPK α:β:γ1-FLAG complexes were immunoprecipitated (*IP*) with anti-FLAG beads and immunoblotted (*WB*) for *O*-GlcNAcylated protein and controls as indicated. Anti-FLAG beads incubated without cell lysate (beads or *B*), and anti-FLAG IPs of cells expressing an empty (α) vector (empty or *em*) were included as negative controls. *C*, wild-type (*WT*), phosphorylated active wild-type (pT172-WT), constitutively active mutant (T172D), or phosphorylated kinase-dead mutant (pT172-K45R) recombinant AMPK α1β1γ1 was incubated with recombinant *O*-GlcNAc transferase (ncOGT) in the presence of UDP-[^{3}H]GlcNAc (an autofluorograph ([^{3}H]GlcNAc; *top panels*) of the same gel stained with G250 Coomassie Blue (Total Protein; *bottom panels*)). Densitometric quantification of *O*-GlcNAcylated γ1 pixel intensities (mean value ± S.E.) were normalized to respective controls. *, **, and *** denote statistical significance of $p < 0.05$, $p < 0.01$, and $p < 0.001$, respectively. #, *12h* time point is representative of one experiment.

no effect on the basal kinase activity of AMPK. Three, although the effect of GT on AICAr-induced increases in α2 activity was not statistically significant, activity of α1 complexes was consistently 8-fold higher than α2 complexes in differentiated C2C12 cells (data not shown).[3] All data using GT has been replicated with TMG, suggesting that all effects discussed above are specific to inhibition of OGA, *versus* off-target effects of either inhibitor used.

In conclusion, our data can be summarized in five main points collectively supporting the potential for ubiquitous cross-talk between the *O*-GlcNAc and AMPK systems in numerous cell lines: 1), nuclear localization of OGT is dynamically regulated by acute metabolic stresses that strongly correlate with AMPK activity, affecting *O*-GlcNAcylation of nuclear proteins and acetylation of K9 on H3 in skeletal muscle myotubes. 2), acute activation of AMPK alters the substrate selectivity of OGT in several proliferating cell lines and the cytoplasm of myotubes. 3), AMPK phosphorylates Thr-444 on OGT *in vitro* and phosphorylation of this residue is associated with AMPK activity and altered nuclear localization and substrate selectivity of OGT. 4), both α- and all 3 γ-subunits of AMPK are dynamically *O*-GlcNAcylated. 5), acute inhibition of *O*-GlcNAc cycling blunts activation of AMPK by physiological and pharmacological stimuli.

DISCUSSION

OGT and AMPK each have a multitude of downstream targets that vary widely based on tissue/cell type and biological or experimental parameters. A better understanding of other orders of regulation that may mediate contextually dependent spatial, temporal, and substrate specific activity of OGT and AMPK, independent of their respective upstream canonical pathways, is needed. Because of the considerable overlap in upstream regulation and downstream functional consequences of OGT and AMPK activity, we wanted to assess the possibility of direct cross-talk between these two enzymes as a novel alternative nutrient-sensitive process that mediates their respective activity and/or substrate specificity. We demonstrated acute regulation of AMPK activity directly correlates with altered nuclear localization of OGT in myotubes, affecting *O*-GlcNAcylation of numerous nuclear proteins and K9 acetylation on H3 (generally associated with transcriptional activation). Our results indicate this could be mediated by direct phosphorylation of Thr-444 on OGT by AMPK. McGee *et al.* demonstrated that AMPK phosphorylates and induces nuclear export of the transcriptional repressor, histone deacetylase 5 (HDAC5), increasing H3 K9Ac levels in differentiated primary human myoblasts (32). Because our data indicate that H3 K9 acetylation is dependent on nuclear localization of OGT in C2C12 myotubes, it would be interesting to investigate if AMPK-induced nuclear export of HDAC5 is dependent on *O*-GlcNAcylation of AMPK, HDAC5, or some other co-activator. Further investigation of how *O*-GlcNAc-dependent regulation of the "histone code" mediates gene transcription in response to processes that regulate AMPK in skeletal muscle (*e.g.* exercise) is a priority for future studies. Such studies could provide vital insight into the molecular mechanisms underlying exercise/mechanical loading-induced global changes in gene transcription that affect skeletal muscle adaptation and plasticity (*e.g.* increased metabolic capacity and/or mass).

Although we observed no effect of AMPK activation on the localization of OGT in proliferating cells, there was a significant effect on the substrate selectivity of OGT in both proliferating cells, and the cytoplasm of myotubes. Our data indicate these effects could also be mediated by phosphorylation of Thr-444 by AMPK. We postulate that the highly distinctive nutritional demand of non-dividing *versus* rapidly dividing cells underscores a potentially unique functional role for OGT in terminally differentiated tissue in general. Consistent with this hypothesis, Whelan *et al.* demonstrated significant nuclear-to-cytoplasmic translocation of OGT upon acute treatment with

[3] All data referenced as "data not shown" have been made accessible for critical review under the same guidelines applied to all data presented in this report.

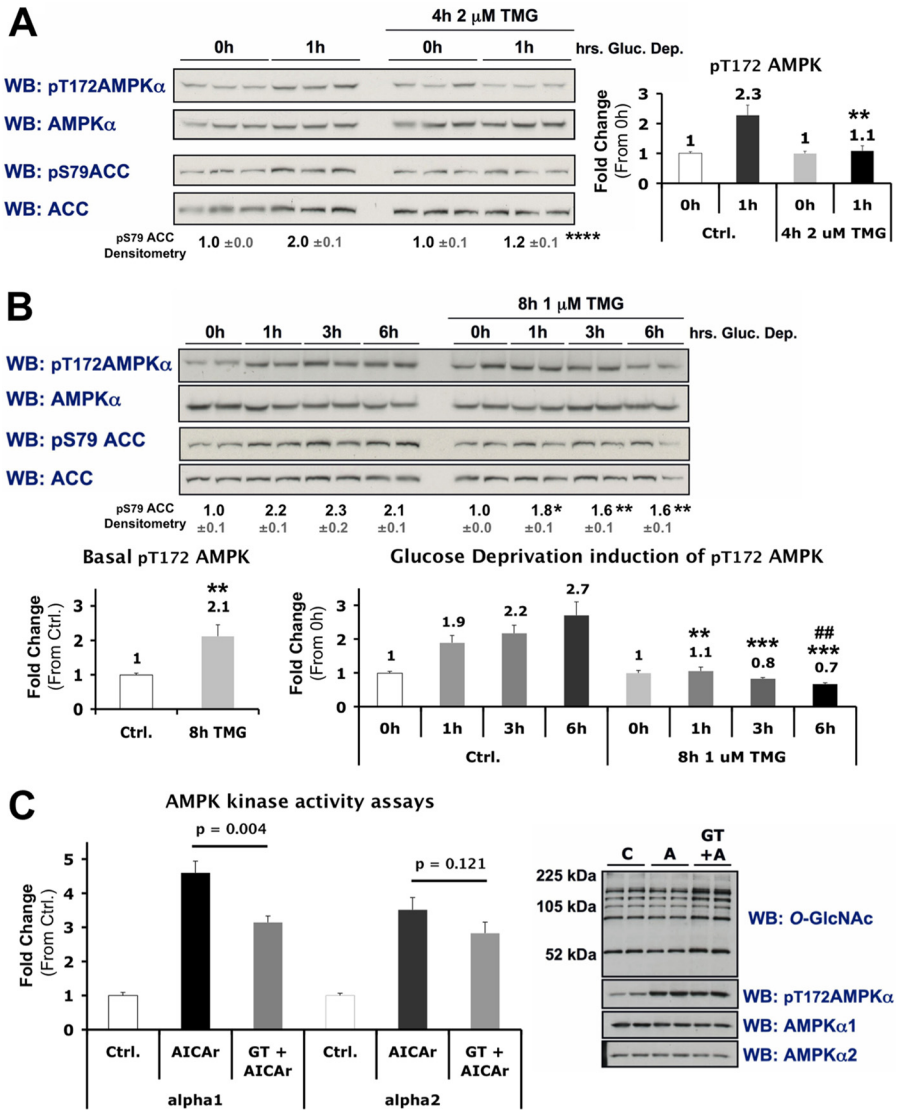

FIGURE 11. **Inhibition of *O*-GlcNAc cycling blunts activation of AMPK in differentiated C2C12 skeletal muscle cells.** *A* and *B*, lysates from differentiated C2C12 cells incubated in 0 mM glucose for 0 or 1 h ± 4 h treatment with TMG (*A*), or 0, 1, 3 or 6 h ± 8 h treatment with TMG (*B*), were immunoblotted (WB) as indicated. Densitometric quantification of phospho- over total AMPK or ACC immunoblots are represented as graphs or *bold numbers* normalized to *Ctrl.*, respectively. *C*, kinase activity assays were performed on AMPK-α1 and -α2 immunoprecipitates of lysates from differentiated C2C12 cells treated with vehicle (*C* or *Ctrl.*), AICAr (*A*; 1 mM, 30 min), or pre-incubated in GT (10 μM, 2 h) prior to AICAr treatment (*GT+A*). *Right panels,* representative control immunoblots of lysate used for kinase activity assays. All quantification represent mean values ± S.E. *, **, ***, and **** denote statistical significance of $p < 0.05$, $p < 0.01$, $p < 0.001$, and $p < 0.0001$, respectively, for *TMG versus Ctrl* for each time point. ## denotes a statistical significance of $p < 0.01$ when comparing the *0h versus 6h* time points in TMG-treated cells.

insulin in differentiated 3T3-L1 adipocytes (26), an effect that is not observed in undifferentiated 3T3-L1 adipocytes or other insulin responsive proliferating cell types. Furthermore, Ramirez-Correa *et al.* demonstrated that *O*-GlcNAcylation of myofilament (cytoplasmic) proteins affects contractile function in cardiac muscle (27), suggesting cytoplasmic OGT may have a distinct functional role in skeletal muscle as well. Collectively, previous publications and our data highlight the broader potential significance for ubiquitous AMPK-mediated regulation of the substrate specificity of OGT in numerous cell types.

To confirm the possibility of cross-talk, we demonstrated AMPK is dynamically *O*-GlcNAcylated on its α- and γ-subunits and acute treatment of cells with inhibitors of OGA blunts activation of AMPK by physiological and pharmacological stimuli. Due to the considerably large number of *O*-GlcNAcylated proteins in a cell, there may be several indirect mechanisms that could account for the effect of acute (2 h) inhibition of OGA on AMPK activation. However, most reported effects of global perturbation of *O*-GlcNAc cycling on various intracellular processes occur on a 6–24 or even 48-h time scale (1). This suggests that the effects we observed are likely due to altered *O*-GlcNAc cycling on AMPK itself. Notably, current tools used to study *O*-GlcNAc in cell culture affect all intracellular *O*-GlcNAcylated proteins, making investigation of the functional role of *O*-GlcNAc on a specific protein quite difficult without the use of site-specific mutant analyses. Due to substoichiometric *O*-GlcNAcylation of recombinant AMPK by ncOGT *in vitro*, and insufficient amounts of material from AMPK immunoprecipitates, current limitations to detection of *O*-GlcNAcylated residues by mass spectrometry (1) have prevented the identification of which residues are *O*-GlcNAc modified on AMPK. Despite these technical caveats, we have dem-

onstrated that highly specific perturbation of *O*-GlcNAc cycling for a short period of time significantly affects activation of AMPK, and that AMPK is dynamically modified by *O*-GlcNAc. Our data imply that global *O*-GlcNAc cycling is important for activation of AMPK, and strengthen the hypothesis of *O*-GlcNAc being a nutrient-sensitive post-translational modification that can regulate AMPK activity independently of AMP/ADP or Ca^{2+}.

In summary, this work establishes a strong foundation for future more targeted interrogation of the potential for OGT and AMPK to participate in synergistic regulation of numerous nutrient-sensitive intracellular processes essential for cellular metabolism, growth, proliferation, and/or tissue function.

Acknowledgments—We thank Chad Slawson, Korin Bullen, and all members of our laboratory for guidance, technical assistance, and critical reading of this manuscript. Dr. Hart receives a share of royalty received by the university on sales of the CTD 110.6 antibody, which are managed by JHU.

REFERENCES

1. Copeland, R. J., Bullen, J. W., and Hart, G. W. (2008) Cross-talk between GlcNAcylation and phosphorylation: roles in insulin resistance and glucose toxicity. *Am. J. Physiol. Endocrinol. Metab.* **295,** E17-E28
2. Hanover, J. A., Krause, M. W., and Love, D. C. (2012) Post-translational modifications: Bittersweet memories: linking metabolism to epigenetics through *O*-GlcNAcylation. *Nat. Rev. Mol. Cell Biol.* **13,** 312–321
3. Hardie, D. G., Ross, F. A., and Hawley, S. A. (2012) AMPK: a nutrient and energy sensor that maintains energy homeostasis. *Nat. Rev. Mol. Cell Biol.* **13,** 251–262
4. Chatham, J. C., Nöt, L. G., Fülöp, N., and Marchase, R. B. (2008) Hexosamine biosynthesis and protein *O*-glycosylation: the first line of defense against stress, ischemia, and trauma. *Shock* **29,** 431–440
5. Kuhajda, F. P. (2008) AMP-activated protein kinase and human cancer: cancer metabolism revisited. *International Journal of Obesity* **32,** S36–S41
6. Slawson, C., and Hart, G. W. (2011) O-GlcNAc signaling: implication for cancer cell biology. *Nat. Rev. Cancer* **11,** 678–684
7. Sakabe, K., and Hart, G. W. (2010) O-GlcNAc transferase regulates mitotic chromatin dynamics. *J. Biol. Chem.* **285,** 34460–34468
8. Hudson, E. R., Pan, D. A., James, J., Lucocq, J. M., Hawley, S. A., Green, K. A., Baba, O., Terashima, T., and Hardie, D. G. (2003) A novel domain in AMP-activated protein kinase causes glycogen storage bodies similar to those seen in hereditary cardiac arrhythmias. *Curr. Biol.* **13,** 861–866
9. Gross, B. J., Kraybill, B. C., and Walker, S. (2005) Discovery of *O*-GlcNAc transferase inhibitors. *J. Am. Chem. Soc.* **127,** 14588–14589
10. Neumann, D., Woods, A., Carling, D., Wallimann, T., and Schlattner, U. (2003) Mammalian AMP-activated protein kinase: functional, heterotrimeric complexes by co-expression of subunits in *Escherichia coli*. *Protein. Expr. Purif.* **30,** 230–237
11. Suter, M., Riek, U., Tuerk, R., Schlattner, U., Wallimann, T., and Neumann, D. (2006) Dissecting the role of 5′-AMP for allosteric stimulation, activation, and deactivation of AMP-activated protein kinase. *J. Biol. Chem.* **281,** 32207–32216
12. Neumann, D., Suter, M., Tuerk, R., Riek, U., and Wallimann, T. (2007) Co-expression of LKB1, MO25α and STRADα in bacteria yield the functional active heterotrimeric complex. *Mol. Biotechnol.* **36,** 220–231
13. Slawson, C., Zachara, N. E., Vosseller, K., Cheung, W. D., Lane, M. D., and Hart, G. W. (2005) Perturbations in *O*-linked β-*N*-acetylglucosamine protein modification cause severe defects in mitotic progression and cytokinesis. *J. Biol. Chem.* **280,** 32944–32956
14. Zeidan Q, Wang, Z., De Maio, A., and Hart, G. W. (2010) *O*-GlcNAc cycling enzymes associate with translational machinery and modify core ribosomal proteins. *Mol. Biol. Cell* **21,** 1922–1936
15. Hardie, D. G., Salt, I. P., and Davies, S. P. (2000) Analysis of the role of the AMP-activated protein kinase in the response to cellular stress. *Methods Mol. Biol.* **99,** 63–74
16. Cheung, W. D., and Hart, G. W. (2008) AMP-activated protein kinase and p38 MAPK activate *O*-GlcNAcylation of neuronal proteins during glucose deprivation. *J. Biol. Chem.* **283,** 13009–13020
17. Graham, D. R., Garnham, C. P., Fu, Q., Robbins, J., and Van Eyk, J. E. (2005) Improvements in two-dimensional gel electrophoresis by utilizing a low cost "in-house" neutral pH sodium dodecyl sulfate-polyacrylamide gel electrophoresis system. *Proteomics* **5,** 2309–2314
18. Li, X., Molina, H., Huang, H., Zhang, Y. Y., Liu, M., Qian, S. W., Slawson, C., Dias, W. B., Pandey, A., Hart, G. W., Lane, M. D., and Tang, Q. Q. (2009) *O*-linked *N*-acetylglucosamine modification on CCAAT enhancer-binding protein β: role during adipocyte differentiation. *J. Biol. Chem.* **284,** 19248–19254
19. Shevchenko, A., Wilm, M., Vorm, O., and Mann, M. (1996) Mass spectrometric sequencing of proteins silver-stained polyacrylamide gels. *Anal. Chem.* **68,** 850–858
20. Udeshi, N. D., Compton, P. D., Shabanowitz, J., Hunt, D. F., and Rose, K. L. (2008) Methods for analyzing peptides and proteins on a chromatographic timescale by electron-transfer dissociation mass spectrometry. *Nat. Protoc.* **3,** 1709–1717
21. Hall, E. H., Balsbaugh, J. L., Rose, K. L., Shabanowitz, J., Hunt, D. F., and Brautigan, D. L. (2010) Comprehensive analysis of phosphorylation sites in Tensin1 reveals regulation by p38MAPK. *Mol. Cell Proteomics* **9,** 2853–2863
22. Geer, L. Y., Markey, S. P., Kowalak, J. A., Wagner, L., Xu, M., Maynard, D. M., Yang, X., Shi, W., and Bryant, S. H. (2004) Open mass spectrometry search algorithm. *J. Proteome. Res.* **3,** 958–964
23. Lazarus, M. B., Nam, Y., Jiang, J., Sliz, P., and Walker, S. (2011) Structure of human *O*-GlcNAc transferase and its complex with a peptide substrate. *Nature* **469,** 564–567
24. Kreppel, L. K., Blomberg, M. A., and Hart, G. W. (1997) Dynamic glycosylation of nuclear and cytosolic proteins. Cloning and characterization of a unique *O*-GlcNAc transferase with multiple tetricopeptide repeats. *J. Biol. Chem.* **272,** 9308–9315
25. Akimoto, Y., Comer, F. I., Cole, R. N., Kudo, A., Kawakami, H., Hirano, H., and Hart, G. W. (2003) Localization of the *O*-GlcNAc transferase and *O*-GlcNAc modified proteins in rat cerebellar cortex. *Brain Res.* **966,** 194–205
26. Whelan, S. A., Lane, M. D., and Hart, G. W. (2008) Regulation of the *O*-linked β-*N*-acetylglucosamine transferase by insulin signaling. *J. Biol. Chem.* **283,** 21411–21417
27. Ramirez-Correa, G. A., Jin, W., Wang, Z., Zhong, X., Gao, W. D., Dias, W. B., Vecoli, C., Hart, G. W., and Murphy, A. M. (2008) *O*-linked GlcNAc modification of cardiac myofilament proteins: a novel regulator of myocardial contractile function. *Circ. Res.* **103,** 1354–1358
28. Sanders, M. J., Ali, Z. S., Hegarty, B. D., Heath, R., Snowden, M. A., and Carling, D. (2007) Defining the mechanism of activation of AMP-activated protein kinase by the small molecule A-769662, a member of the thienopyridone family. *J. Biol. Chem.* **282,** 32539–32548
29. Shen, D. L., Gloster, T. M., Yuzwa, S. A., and Vocadlo, D. J. (2012) Insights into *O*-linked *N*-acetylglucosamine (O-GlcNAc) processing and dynamics through kinetic analysis of *O*-GlcNAc transferase and *O*-GlcnAcase activity on protein substrates. *J. Biol. Chem.* **287,** 15395–15408
30. Whitworth, G. E., Macauley, M. S., Stubbs, K. A., Dennis, R. J., Taylor, E. J., Davies, G. J., Greig, I. R., and Vocadlo, D. J. (2007) Analysis of PUGNAc and NAG-thiazoline as transition state analogues for human O-GlcNAcase: mechanistic and structural insights into inhibitor selectivity and transition state poise. *J. Am. Chem. Soc.* **129,** 635–644
31. Yuzwa, S. A., Macauley, M. S., Heinonen, J. E., Shan, X., Dennis, R. J., He, Y., Whitworth, G. E., Stubbs, K. A., McEachern, E. J., Davies, G. J., and Vocadlo, D. J. (2008) A potent mechanism-inspired O-GlcNAcase inhibitor that blocks phosphorylation of tau *in vivo*. *Nat. Chem. Biol.* **4,** 483–490
32. McGee, S. L., van Denderen, B. J., Howlett, K. F., Mollica, J., Schertzer, J. D., Kemp, B. E., Hargreaves, M. (2008) AMP-activated protein kinase regulates GLUT4 transcription by phosphorylating histone deacetylase 5. *Diabetes* **57,** 860–867